AD-A123 224 SYNTHESIS AND PROPERTIES OF ELEVATED TEMPERATURE P/M ALUMINUM ALLOYS(U) NORTHWESTERN UNIV EVANSTON IL DEPT OF MATERIALS SCIENCE AND E.. M E FINE ET AL. 29 NOV 82 1/1

UNCLASSIFIED AFOSR-TR-82-1062 AFOSR-82-0005 F/G 11/6 NL

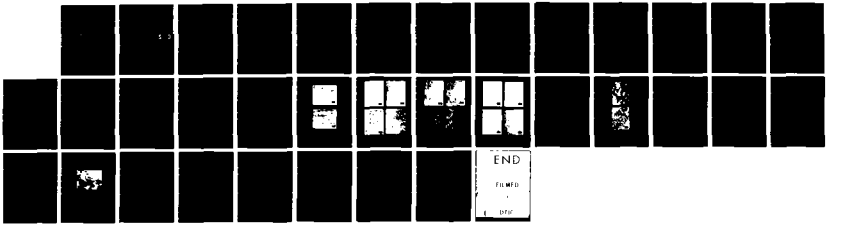

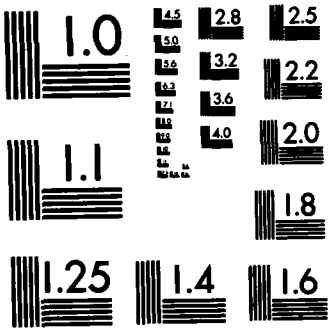

SECURITY CLASSIFICATION OF THIS PAGE (When Data Entered)

REPORT DOCUMENTATION PAGE

READ INSTRUCTIONS BEFORE COMPLETING FORM

1. REPORT NUMBER	2. GOVT ACCESSION NO.	3. RECIPIENT'S CATALOG NUMBER
AFOSR-TR- 82-1062	AD-A123224	

4. TITLE (and Subtitle)

SYNTHESIS AND PROPERTIES OF ELEVATED TEMPERATURE P/M ALUMINUM ALLOYS

5. TYPE OF REPORT & PERIOD COVERED

Annual Technical Report
10/1/81 - 9/30/82

6. PERFORMING ORG. REPORT NUMBER

7. AUTHOR(s)

Morris E. Fine
Julia R. Weertman

8. CONTRACT OR GRANT NUMBER(s)

AFOSR-82-0005

9. PERFORMING ORGANIZATION NAME AND ADDRESS

Northwestern University
Dept. of Materials Science & Engineering
Evanston, Illinois 60201

10. PROGRAM ELEMENT, PROJECT, TASK AREA & WORK UNIT NUMBERS

2306/A1
61102F

11. CONTROLLING OFFICE NAME AND ADDRESS

Air Force Office of Scientific Research/NE
Bolling AFB, Building 410
Washington, D. C. 20332

12. REPORT DATE

11/29/82

13. NUMBER OF PAGES

31

14. MONITORING AGENCY NAME & ADDRESS (if different from Controlling Office)

15. SECURITY CLASS. (of this report)

Unclassified

15a. DECLASSIFICATION/DOWNGRADING SCHEDULE

16. DISTRIBUTION STATEMENT (of this Report)

Approved for public release;
distribution unlimited.

DTIC
ELECTE
JAN 7 1983
S D
B

17. DISTRIBUTION STATEMENT (of the abstract entered in Block 20, if different from Report)

18. SUPPLEMENTARY NOTES

19. KEY WORDS (Continue on reverse side if necessary and identify by block number)

Ostwald ripening (coarsening), aluminum-iron cerium alloys, aluminum-titanium-zirconium-hafnium alloys

20. ABSTRACT (Continue on reverse side if necessary and identify by block number)

In dispersion strengthened high temperature alloys the particle radius is theoretically predicted to be proportional to $(\sigma D C_o t)^{\frac{1}{3}}$ where σ is the interfacial energy, D, the diffusivity, C_o the solubility limit and t is time. Thus, information about σ, D, and C_o are needed to design and evaluate high temperature alloys. The Al-8Fe-3Ce alloy developed by Alcoa Research Center is being studied on this basis. Assuming diffusion of iron is rate controlling, values of σ are calculated indicating an incoherent interface; however, the coarsening is more complex than predicted by the simple theory. Low values of σ are expected when

DD FORM 1 JAN 73 1473 EDITION OF 1 NOV 65 IS OBSOLETE

UNCLASSIFIED

SECURITY CLASSIFICATION OF THIS PAGE (When Data Entered)

20. (continued)

there is good lattice matching across the interface. $Al_3(Ti,Zr,Hf)$ is being studied seeking good lattice matching. $Al_3(Ti,Zr)$, $Al_3(Ti,Hf)$, $Al_3(Zr,Hf)$ have been studied to date and the best matching is obtained with $Al_3((Ti_{0.75}Zr_{0.25})$ where the lattice mismatch between the compound and aluminum is 3-4%.

DEPARTMENT OF MATERIALS SCIENCE & ENGINEERING
THE TECHNOLOGICAL INSTITUTE
NORTHWESTERN UNIVERSITY
EVANSTON, ILLINOIS

Annual Technical Report on

Synthesis and Properties of Elevated Temperature P/M Aluminum Alloys

AF Grant No.: AFOSR-82-0005

For the Period
1 October 1981 to 30 September 1982

Principal Investigators:

Morris E. Fine, Walter P. Murphy Professor of Materials Science and Engineering (Telephone: (312) 492-5579)

Julia R. Weertman, Professor of Materials Science and Engineering (Telephone: (312) 492-5353)

November 29, 1982

The objective of this research is to provide basic data needed to design a high temperature aluminum base alloy useful to 375° C.

According to the Wagner-Lifshitz-Slyozov (W-L-S) theory for diffusion controlled coarsening of a dispersed phase the average radius at time t, $\bar{r}_t$ is proportional to $(\sigma DC_o t)^{\frac{1}{3}}$ where σ is the interfacial energy, D is the diffusivity of the rate controlling element, and C_o is the solubility limit. For microstructural stability at high temperatures, the dispersed phase must be thermodynamically stable, and the product σDC_o must be small. Thus information about σ, D, and C_o are needed as the basis for design of Al alloys for elevated temperature use. If D and C_o are known, then measurement of $\bar{r}_t$ vs. t at constant temperature gives σ. Low values of σ are expected when there is good lattice matching across the interface between dispersed phase and matrix.

During the past year two topics were under study:

1. Determination of $\bar{r}$ vs. t for the dispersed phase in the elevated temperature alloy nominal composition Al-8Fe-3Ce alloy developed by Alcoa Research Center. Since the dispersed phase has not yet been identified, studies to this end were also undertaken.
2. Determine lattice parameters of Al_3 (Ti, Zr, Hf) compared to aluminum solid solution seeking interfacial matching and low σ.

1. Studies of Al-Fe-Ce Alloy

a. Coarsening kinetics of RSP P/M Al-7.5Fe-3.4Ce alloy during exposure to high temperatures

For the studies on the RSP P/M Al-Fe-Ce alloy, a quantity containing 7.5 wt.% Fe and 3.4 wt.% Ce was obtained in the form of upset forged pancakes from the Air Force Materials Laboratory, Wright-Patterson Air Force Base. Small pieces of the material were aged, in a vacuum of $\sim 8 \times 10^{-8}$ torr, at

375°, 475°, or 575°C, for varying lengths of time. The longest heat treatments lasted 120 hours. The aged specimens were polished and etched slightly in an 0.05% aqueous solution of HF to bring out the microstructure. Coarsening measurements were made from TEM micrographs of shadowed two stage replicas of the specimen surfaces. Point counting[1] was used to determine the volume fraction taken up by the precipitates. For each value of volume fraction, 2000 grid points were used. The total surface area of the precipitates was obtained by measuring the number of intersections of the precipitates with grid lines. Approximately 2200 μm of grid lines were scrutinized for each surface area measurement. A mean intercept length, $\bar{L}$, was determined from the surface area and volume fraction for each pair of values of the temperature and aging time. If the particles are spherical (and they appear to be roughly so at 575°C), the mean intercept length is an effective measure of precipitate diameter but at all times its value will be less than the actual diameter. To obtain size distributions, particle intercept lengths on random test lines were measured for over 400 particles for each histogram.

Figure 1 shows the microstructure of the Al-Fe-Ce alloy in the as received condition. The optical micrographs were taken parallel and perpendicular to the direction of forging. Figure 2 shows a series of TEM micrographs of samples aged at 575°C for varying lengths of time. Similar series of samples aged at 475°C and 375°C are presented in Figs. 3 and 4. It can be seen that the size distribution is very inhomogeneous. (Precipitation at 375°C is too heterogeneous for satisfactory measurements of particle ripening. For example, a considerable amount of precipitation at grain boundaries is observed.) The results of the measurements of particle coarsening are given in Figs. 5 and 6. Straight lines with slope of 0.33

have been drawn through the points, to conform with the predictions of the Wagner-Lifschitz theory. While the line determined by a least squares fit of the data points at 575° C has a somewhat lower slope, the agreement with the 0.33 value is not unreasonable. Preliminary calculations have been made of the energy of the interface between precipitate and matrix. The literature has been surveyed for values of the diffusivity D of Fe and Ce in Al, as well as for the other material constants appearing in the Wagner-Lifschitz equation. There is a wide range in the values reported for D. The following table lists values calculated for the interfacial energy σ from the coarsening data at 575° C and the Wagner-Lifschitz equation:

$$\sigma = \frac{9}{64} \frac{\bar{d}^3}{t} \frac{kT}{DC\Omega}$$

where $\bar{d}$ is the average precipitate diameter at time t, T is the absolute temperature, D is the appropriate lattice diffusion coefficient, C is the solubility limit of Fe or Ce in Al, Ω is the atomic volume and k is Boltzmann's constant.

Table 1. Values of the interfacial energy/cm^2 σ between matrix and Al-Fe-Ce precipitate in Al-7.5Fe-3.4Ce. Interfacial energy is measured at 575° C.

D cm^2/sec	reference for D measurement	σ ergs/cm^2
$9.1\times10^{6} e^{\frac{-31.0\times10^3}{T}}$	G. M. Hood Phil. Mag. 21 (1970) 305	1,130
$0.12 e^{\frac{-16.2\times10^3}{T}}$	K. Sorensen and G. Trumpy Phys. Rev. B1 7 (1973) 1791	222
$135 e^{\frac{-23.2\times10^3}{T}}$	W. B. Alexander, L. M. Slifkin Phys. Rev. B1 8 (1970) 3274	667
$4.1\times10^{-9} e^{\frac{-6.95\times10^3}{T}}$	K. Hirano, R. P. Agarwala, M. Cohen Acta Met. 10 (1962) 857	117,060

While there is a wide spread in σ, the more recent reported values for the

diffusivity of Fe in Al lead to surface energies which are reasonable. The energies calculated from the ripening data at 475° C appear to be too high. (It should be noted, however, that many of the particles at 475° C are plate-like rather than spherical. Furthermore, data taken to date contain large statistical errors. Additional measurements are needed to determine the average particle size as a function of time at 475° C.) The cerium diffusivities also give values for σ which are unreasonably large. This last fact would seem to indicate that Fe diffusion is controlling and that the precipitates might change their composition and homogeneity as they ripen.

In Fig. 7, TEM micrographs of thin foils aged at 475° C and 575° C are presented to illustrate the dependence of morphology on aging temperature. While the particles in the foil aged at 575° C are more or less spherical, the particles in the foil aged at 475° C often appear to be plate-like with no preferred orientation.

Figures 8 and 9 show the evolution in the distribution of precipitate size produced by aging the samples at 575° C and 475° C. Here L is intercept length of a particle and f(L) is the fraction of particles with intercepts in the size range around L. While at short times the histograms appear to follow the initial narrow Gaussian distribution expected, there is no evidence of the asymmetric (skewed to the right) steady state solution for long coarsening times. Figures 10 and 11 show the size distributions with the intercept length normalized by dividing each intercept length by the mean intercept length $\bar{L}$. The Wagner-Lifschitz theory requires that the distribution is cut off when the value of $L/\bar{L}$ is equal to 1.5. It has been shown[2] that this value may be as high as 2.0 for systems with such high volume fraction as ours. However, in all measurements

on this alloy, particles whose intercept length is up to seven times the average have been found to exist. This result may indicate that coalescence is occurring, that there are two or more distinct phases which are coarsening at different rates, or that the precipitates are not merely coarsening but changing composition.

b. Identification of precipitates in the P/M Al-7.5Fe-3.4Ce alloy

It has been suggested[3] that the precipitates in the Al-Fe-Ce alloy may be either of the ternary intermetallic phases, Al_8Fe_4Ce or $Al_{10}Fe_2Ce$, and that the matrix is free of Fe and Ce.

A bulk specimen of the alloy was prepared for x-ray diffraction. The specimen aged for 120 hours at 575° C was chosen because the precipitates were large enough that a significant signal would be obtained from the precipitate as well as the matrix. From the diffraction pattern, the aluminum peaks were identified and the lattice parameter was calculated to be about 0.25% larger than that of pure aluminum, indicating the presence of some iron and/or cerium in solid solution. The remaining peaks, contributed by the second phase, did not correspond to lattice spacings of either $FeAl_3$ or Al_8Fe_4Ce. A search of the literature yielded no crystallographic information on $Al_{10}Fe_2Ce$ and hence it was not possible to determine whether the remaining peaks come from this phase or not. The same set of diffraction peaks was found when studying a bulk specimen which had been aged at 475° C for 24 hours.

Chemical analysis was performed by semi-quantitative energy dispersive spectrometry in a scanning transmission electron microscope. Figure 12 shows a thin foil of the Al-Fe-Ce alloy in the as-received condition. A full screen analysis, corresponding to an area 10 μm by 10 μm,

indicated a composition of 91.03 wt.% Al, 6.70% Fe, 2.27% Ce, compared to the nominal 89.1 wt.% Al, 7.5% Fe, 3.4% Ce. The difference between these compositions is negligible since the alloy is not very homogeneous on this fine a scale. Analysis over a number of points would likely average out to the nominal composition. (Analysis over a larger area is not feasible, due to instrumental limitations.) Upon condensing the beam into a spot in the matrix, as in A, chemical analysis revealed approximately 1.7 weight percent Fe and essentially no Ce.

Chemical analysis of the precipitates by means of energy dispersive spectrometry in the STEM is continuing. Efforts are underway to prepare extraction replicas using etchants which do not alter the composition of the precipitates.

c. Effect of plastic deformation on coarsening kinetics in the P/M Al-7.5Fe-3.4Ce alloy

Some tests have been conducted to study the enhancement of coarsening rates by creep. The deformation is carried out in argon at elevated temperatures. The geometry of the creep specimen, prepared by electric discharge machining, is shown in Fig. 13. Specimens were first brought to temperature and held for one hour before loading. The specimens then were crept for the remaining time and compared with specimens aged under no load. At 475° C and 1000 psi, replicas were taken after 12 hour and 24 hour tests. Both specimens had crept to a final strain of about 6%. There was no startling enhancement of the coarsening kinetics as can be seen in the table below.

Table 2. Mean intercept length for coarsening at 475° C

	No load	1000 psi
12 hour	0.19 μm	0.20 μm
24 hour	0.17	0.24

The size distributions are presented in Fig. 14.

Because at very high temperatures the equilibrium concentration of vacancies is much larger than the additional concentration of vacancies produced by plastic deformation, one may expect the change in coarsening kinetics to be insignificant. At lower temperatures, the vacancy concentration due to plastic deformation is a more significant contribution and the coarsening kinetics may be enhanced. At 375° C and 2500 psi, 12 hour and 24 hour tests were performed to final strains of 5.4%. The microstructures observed were very inhomogeneous and could not be analyzed in the manner as above. Longer tests at higher stress amplitudes are in progress.

2. Lattice Parameters of Al_3(Zr, Ti, Hf)

A high-temperature dispersion strengthened aluminum base alloy containing Al_3Ti[5], as the dispersed phase, has been proposed.[4] The lattice parameters of tetragonal Al_3Ti[2], a' and c, are very close to a_o and $2a_o$, respectively, where a_o is the lattice parameter of cubic Al and a' is the half diagonal length of the (001) plane in a unit cell of Al_3Ti; a' is 5% less than a_o, and c is 6% more than $2a_o$ (Table 3). It was suggested that suitable alloying might reduce this mismatch and thereby reduce the interfacial energy and the coarsening rate of dispersed Al_3Ti particles in an aluminum matrix, improving the elevated temperature fatigue and creep resistance.

The intermetallic compounds Al_3Zr[5] and Al_3Hf[6] may be more promising than Al_3Ti. They are structurally similar to Al_3Ti[5], space group D_{4h}^{17} apart from a modulation along the c-axis. The lattice parameter, a, is only 1% less than a_o of aluminum for both (Table 1); however, the mismatch in the c directions are 5 to 7%. Thus it seemed likely that there would be

extensive solid solubility of Zr and Hf in Al_3Ti and vice versa with the possibility of obtaining an intermetallic compound solid solution with smaller mismatch to the lattice parameters of the aluminum matrix.

It was, therefore, decided to investigate the phase relations in the Al-Ti-Zr-Hf system and how the lattice parameters of $Al_3(Zr_{(x)}Ti_{(y)}Hf_{(z)})$ vary with x and y and z (x+y+z=1).

Table 3. Comparison of the lattice parameters of Al, Al_3Ti, Al_3Zr and Al_3Hf

Compound	Ref.	Structure	Lattice Parameters in nm and Their Ratios			
Al		cubic	a_o=.405			
Al_3Ti	5	tetragonal	a=.543 $a'=\frac{a}{\sqrt{2}}$=3.84	a'/a_o=0.95	c=.860	$/2a_o$=1.06
Al_3Zr	5	tetragonal	a=.401	a/a_o=0.99	c=1.715	$4a_o$=1.07
Al_3Hf	6	tetragonal	a=.399	a/a_o=0.99	c=1.715	$4a_o$=1.05

To date the Al-Zr-Ti, Al-Zr-Hf, and Al-Ti-Hf systems have been investigated.

Experimental

Small, approximately 5 gram, Al-2 at.% (Zr,Ti,Hf) alloy buttons were made in a gettered argon atmosphere by arc melting. The Al was 99.996% pure, the Ti was Johnson-Matthey spectrochemical grade, and Zr and Hf were cut from crystal bars prepared by the van Arkel process. Each button was melted four to five times, inverted between each melting to ensure homogeneity, and then annealed for 24 hours at 475° C. Twenty-one ternary compositions were prepared. The presence of large intermetallic compound particles were verified by optical metallography.

For X-ray analyses, the buttons were powdered with an automatic filing machine, and the fraction passing through a 150-mesh screen was used. The

specimen powders were annealed at 300°C and mixed with Si powder for standardizing the determination of the peak positions. The diffraction data were obtained with CuKα radiation in a Rigaku "Geigerflex" D/Max-IIA X-ray diffractometer.

Results

Al-Ti-Zr System

The a and c lattice parameters of $Al_3(Zr_xTi_{1-x})$ compared to a_o for the Al(SS) are shown in Figs. 16a and b, where the open circles are the results for the present alloys. The closed circles are JCPDS data for Al_3Ti and Al_3Zr, cards #2-1121 and 2-1093, respectively, which were taken from reference (5), while the triangles are the lattice parameters of an Ar atomized Al-4.7 at.% Ti alloy powder. The almost horizontal dotted line in Fig. 16a represents the cubic lattice parameters of the Al solid solutions, $a_o(SS)$, obtained from the X-ray data. It is very nearly equal to the a_o of Al, showing that almost all Ti and Zr are always present in the $Al_3(Zr_xTi_{1-x})$. For Al_3Ti $a/\sqrt{2}$ is plotted rather than a. In Fig. 16b the dotted line is four times $a_o(SS)$. Also, 2c is plotted for $Al_3Ti(SS)$ rather than c for better comparison with c of the $Al_3Zr(SS)$.

Only Al_3Ti-type diffraction patterns were observed in the specimens, Al-2.0 at.% Ti to Al-1.78 at.% Ti-0.22 at.% Zr (i.e., x = 0 and 0.11). Only the Al_3Zr-type diffraction patterns were observed in the specimens, Al-1.51 at.% Ti-0.49 at.% Zr, Al-1.02 at.% Ti-0.98 at.% Zr, Al-0.51 at.% Ti-1.49 at.% Zr and Al-2.0 at.% Zr (i.e., x = 0.25, 0.49, 0.75 and 1, respectively).

The parameters of Al_3Ti, a = .5449 ± .0003 nm ($a' = a/\sqrt{2}$ = .3853 ±

.0002 nm) and c = .8618 ± .0005 nm determined in both the arc melted Al-2.0 at.% Ti and Ar atomized Al-4.7 at.% Ti alloys are larger by at most .002 nm than those of Al_3Ti alone, while the lattice parameters of Al_3Zr, a = .4014 ± .0001 nm and c = 1.7315 ± .0005 nm in Al-2.0 at.% Zr are in good agreement with those of Al_3Zr alone within experimental error. As shown by the X-ray patterns and the discontinuity in the a and c data near x = 0.2, two ranges of solid solution exist in the Al_3Ti-Al_3Zr system. Both intermetallic compound solid solutions, that is solid solutions derived from Al_3Ti and Al_3Zr, exist in a region between x = 0.11 and 0.25.

While addition of Ti to Zr slightly increases the mismatch of a of Al_3Zr(SS) to a_o of aluminum, the mismatch in the c lattice spacing is much reduced, the least being for the x = 0.25 alloy where the mismatch in c is 4%. For this alloy the mismatch in a is about 3%.

Al-Ti-Hf System

Similar data to the above for $Al_3(Hf_yTi_{1-y})$ are presented in Figs. 17a and b. Again the closed circles are JCPDS data for Al_3Ti and Al_3Hf, card 13-512[8] for the latter. Again a_o for the Al(SS) is very close to that for Al showing very little solid solubility of Hf or Ti in Al. There is a discontinuity in a and c values between y = 0 and 0.12 indicating the existence of a two phase field. The c mismatch is least for $Al_3(Hf_{.12}Ti_{.88})$ being 5% with $4a_o$. The a/a_o mismatch for this composition is 2.5%.

Al-Zr-Hf System

The a and c lattice parameters for $Al_3(Zr_zHf_{1-z})$ are shown in Figs. 18a and 18b. Again a_o and $4a_o$ of the Al(SS) are plotted for comparison. For this system Al_3Zr and Al_3Hf appear to form a complete series of solid

solutions. The lattice parameters essentially obey Vegard's rule. The mismatch of c with $4a_o$ is least for Al_3Hf.

Discussion

In all cases the measured values of a and c for Al_3Ti, Al_3Zr and Al_3Hf are in good agreement with JCPDS compiled data as shown by comparison of the open and closed circles in Figs. 16-18.

The psuedo-ternary phase diagram Al_3Ti-Al_3Zr-Al_3Hf shows a two-phase region approximately as indicated in Fig. 19. This diagram probably holds for temperatures up to near the liquidus. The designation Al_3Ti(SS) refers to a solid solution having the Al_3Ti structure while $Al_3\{Zr,Hf\}$(SS) refers to a solid solution having the Al_3Zr and Al_3Hf structure.

While adding Ti to Al_3Zr or Al_3Hf increases the mismatch of the a lattice parameter with a_o for the Al(SS) the mismatch of c with $4a_o$ of the Al(SS) is improved. The least mismatch for Ti in Al_3Zr-Al_3Ti or Al_3Hf-Al_3Ti occurs with the maximum Ti allowable without forming the "Al_3Ti(SS)" phase. In spite of the fact that c for Al_3Hf matches $4a_o$ of the Al(SS) better than Al_3Zr, Ti has a larger effect on c of Al_3Zr so the best matching occurs in this system.

From the lattice mismatch point of view the best alloys for obtaining a low interfacial energy between the intermetallic compound and the matrix obtained so far are shown in Table 4.

Table 4. Al-Ti-Zr-Hf intermetallic compounds demonstrating minimum lattice mismatch

	a	c	a/a_o	$c/4a_o$
Al-$Al_3(Ti_{.87}Hf_{.13})$	0.395 nm	1.699 nm	0.98	1.05
Al-$Al_3(Ti_{.75}Zr_{.25})$	0.394	1.684	0.97	1.04

References

1. E. E. Underwood, Quantitative Stereology, Addison-Wesley, 1970.

2. A. J. Ardell, "The Effect of Volume Fraction on Particle Coarsening: Theoretical Considerations", Acta Met. 20, 61 (1972).

3. R. E. Sanders, Jr., G. J. Hildeman and F. G. Nelson, "Elevated Temperature Al Alloy Development", Technical Report, AFML Contract No. F33615-77-C-5086, July 31, 1980.

4. M. E. Fine, "Precipitation Hardening of Aluminum Alloys", Met. Trans. A 6, 625 (1975).

5. G. Brauer, "Uber die Kristallstruktur von $TiAl_3$, NbA_3, $TaAl_3$ and $ZrAl_3$", Z. anorg. allg. Chem. 242, 1 (1939).

6. B. Dwight et al., "Some AB_3 Compounds of the Transition Metals", Acta Cryst. 14, 75 (1961).

LIST OF PUBLICATIONS -- AF SUPPORTED

M. E. Fine

1. "Lattice Parameters of $Al_3(Zr_xTi_{1-x})$ vs. x in Al-2 at.% (Ti+Zr) Alloys" (with S. Tsunekawa), Scripta Met. 16, 391 (1982).

2. "Effect of Purity and Dispersoid Type on Near Threshold Fatigue Crack Growth Rates in Al-Zn-Mg-Cu Alloys" (with M. Zedalis and L. Filler), Scripta Met. 16, 471 (1982).

3. "Fatigue Crack Initiation and Microcrack Propagation in X7091 Type Aluminum P/M Alloys" (with S. Hirose), Proceedings of Symposium on Powder Metallurgy of Aluminum Alloys, AIME Annual Meeting, Dallas, TX, February 1982 (in press).

4. "The Effect of Aluminum Oxide Particles and Precipitate Type on Near-Threshold Fatigue Crack Propagation Rate in P/M 7XXX Aluminum Alloys" (with M. Zedalis), Scripta Metallurgica (in press).

J. R. Weertman

1. "Void Nucleation in Astroloy: Theory and Experiments" (with M. Kikuchi and K. Shiozawa), Acta Met. 29, 1747-1758 (1981).

2. "Observation of Grain Boundary Microcracking in a Nickel Base Superalloy after Room Temperature Deformation" (with K. Shiozawa), Scripta Met. 15, 1241-1244 (1981).

3. "Nucleation of Grain Boundary Voids in the Vicinity of an Intergranular Fatigue Crack" (with B. Kirkwood), Scripta Met. 16, 627-632 (1982).

4. "The Nucleation of Grain Boundary Voids in Astroloy During High Temperature Creep" (with K. Shiozawa), Scripta Met. 16, 735-739 (1982).

5. "Cavity Nucleation during Fatigue Crack Growth Caused by Linkage of Grain Boundary Cavities" (with B. Kirkwood), Micro and Macro Mechanics of Crack Growth, edited by K. Sadananda, D. J. Michel and B. B. Rath, TMS-AIME, 1982.

6. "Deformation-Induced Strain Localization and Residual Stresses around Hard Particles" (with K. Shiozawa), Proceedings of Workshop on Plasticity of Metals at Finite Strain, June 29-July 1, 1981, Stanford University (in press).

7. "Studies of Nucleation Mechanisms and the Role of Residual Stresses in the Grain Boundary Cavitation of a Superalloy" (with K. Shiozawa), Acta Metallurgica (in press).

PAPERS AND TALKS PRESENTED -- AF SUPPORTED

J. R. Weertman

1. "Cavity Nucleation during Fatigue Crack Growth Caused by Linkage of Grain Boundary Cavities", B. Kirkwood and J. R. Weertman, AIME/TMS Fall Meeting, Louisville, KY, October 15, 1981.

2. "Strain Induced Microcracking at Inclusions: Theory and Experiments", Colloquia in Metallurgy, Exxon Research and Engineering Co., Corporate Research Science Lab, Linden, NJ, November 6, 1981 (invited).

3. "Fatigue Crack Propagation by Grain Boundary Void Coalescence", University of Wisconsin/Milwaukee, Milwaukee, WI, December 10, 1981 (invited).

4. "Fatigue Crack Growth by Linkage of Grain Boundary Cavities", Department of Ceramics, University of Illinois, Urbana, IL, January 29, 1982 (invited).

5. "Cavity Nucleation during Fatigue Crack Growth", Oak Ridge National Laboratory, Oak Ridge, TN, April 8, 1982 (invited).

6. "Void Nucleation and Growth in Metals and Alloys", Alcoa Technical Center, Pittsburgh, PA, June 4, 1982 (invited).

M. E. Fine

1. "Fatigue Crack Initiation and Propagation in MA87 and Related Alloys", AFML Aluminum Alloy Powder Metallurgy Conference, Louisville, KY, October 15, 1981 (invited).

2. "Fatigue Crack Initiation and Microcrack Propagation in X7091 P/M Type Aluminum Alloys", S. Hirose and M. E. Fine (presented by M. E. Fine), AIME Annual Meeting, Dallas, TX, February 1982.

PROFESSIONAL PERSONNEL

1. Professor Morris E. Fine, Principal Investigator

2. Professor Julia R. Weertman, Principal Investigator

3. Dr. Shin Tsunekawa, Visiting Postdoctoral Fellow 10/1/81-12/15/81.

4. Mr. Michael S. Zedalis, Ph.D. student.

5. Ms. Lynette Angers, Ph.D. student.

(a)

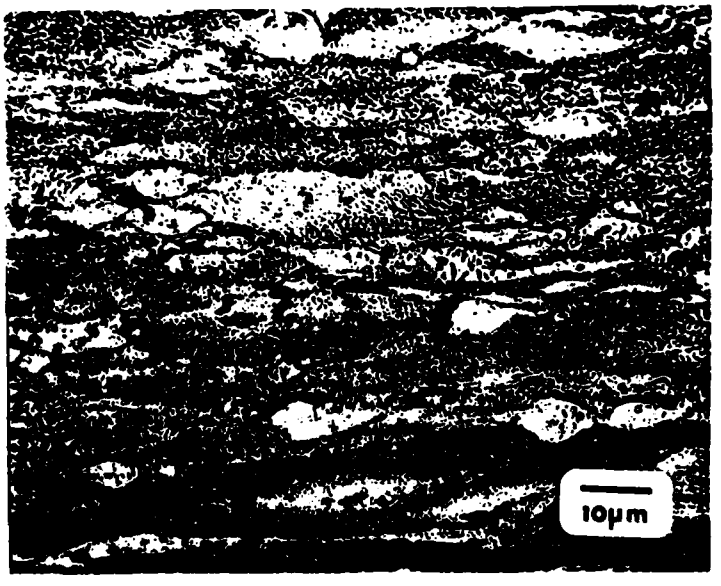

(b)

Fig. 1. Microstructure of the Al-7.5Fe-3.4Ce alloy in the as-received condition. (a) section perpendicular to the upsetting direction, (b) section parallel to the upsetting direction.

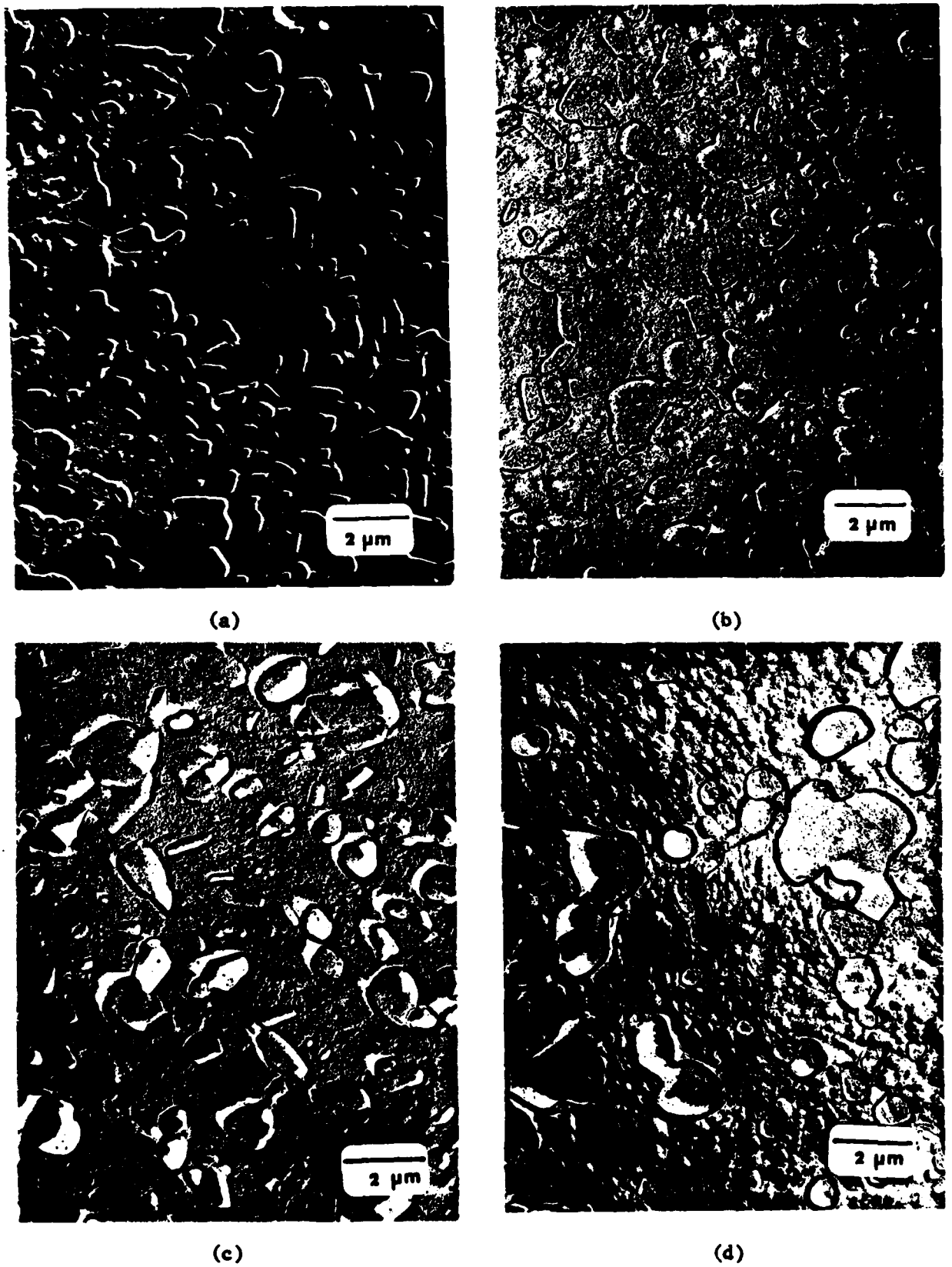

Fig. 2. Series of TEM micrographs of replicas of samples aged at 575°C in vacuum of 8×10^{-6} torr. (a) aged 2 hrs, (b) 12 hrs, (c) 24 hrs and (d) 120 hrs.

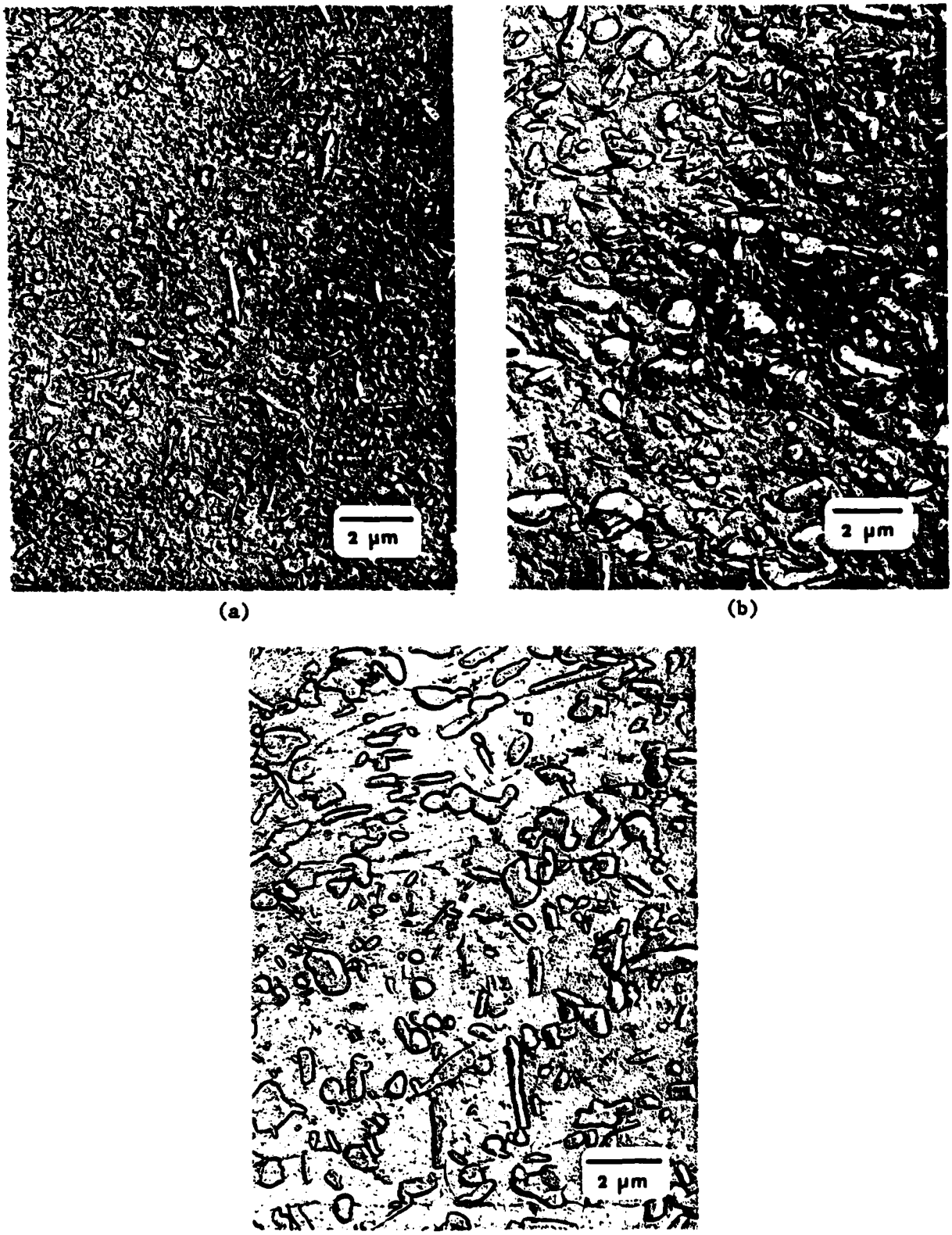

Fig. 3. Series of TEM micrographs of replicas of samples aged at 475°C in vacuum of 8×10^{-8} torr. (a) aged 2 hrs, (b) 12 hrs and (c) 24 hrs.

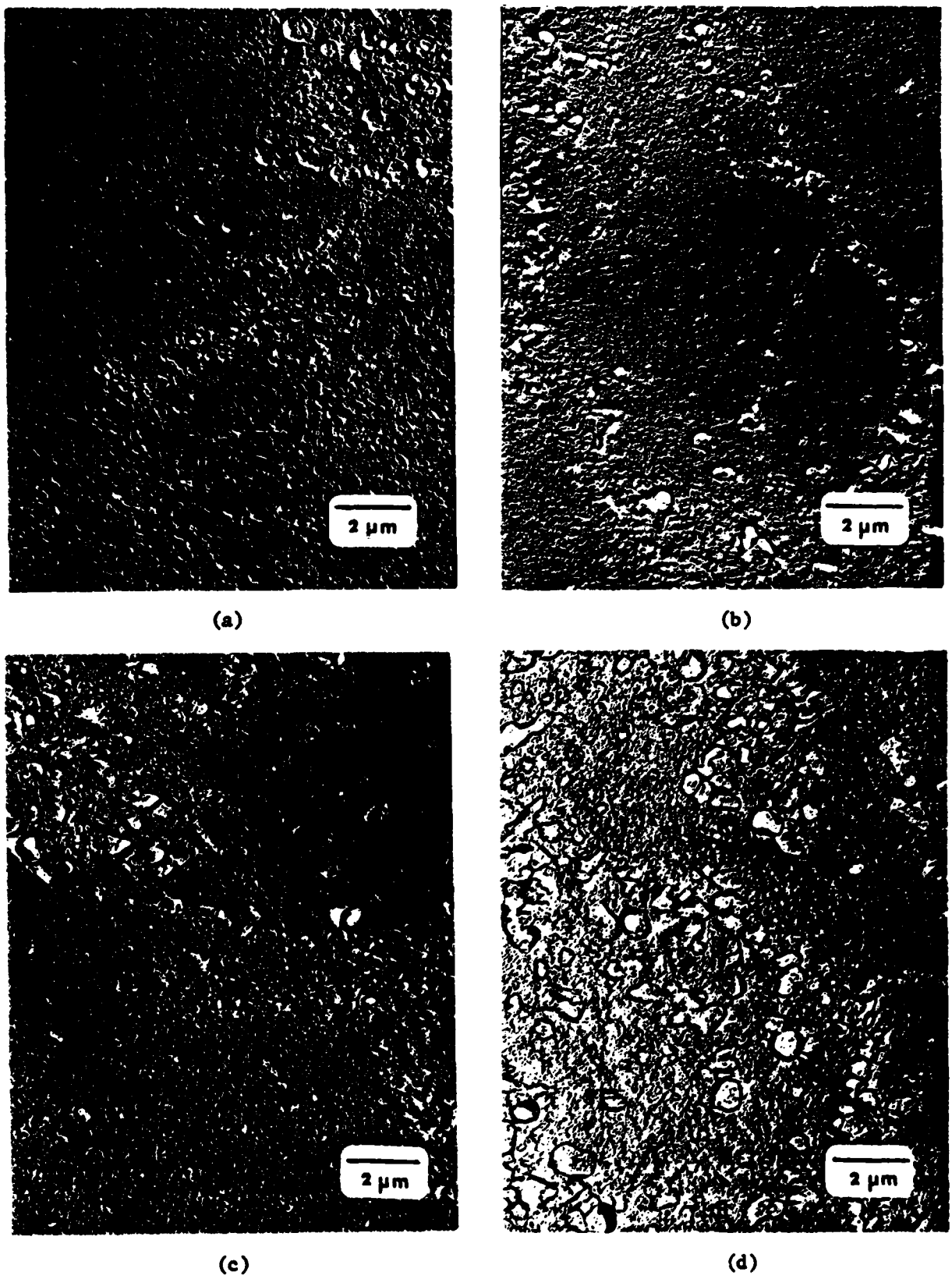

Fig. 4. Series of TEM micrographs of replicas of samples aged at 375°C in vacuum of 8×10^{-6} torr. (a) aged 2 hrs, (b) 12 hrs, (c) 24 hrs and (d) 120 hrs.

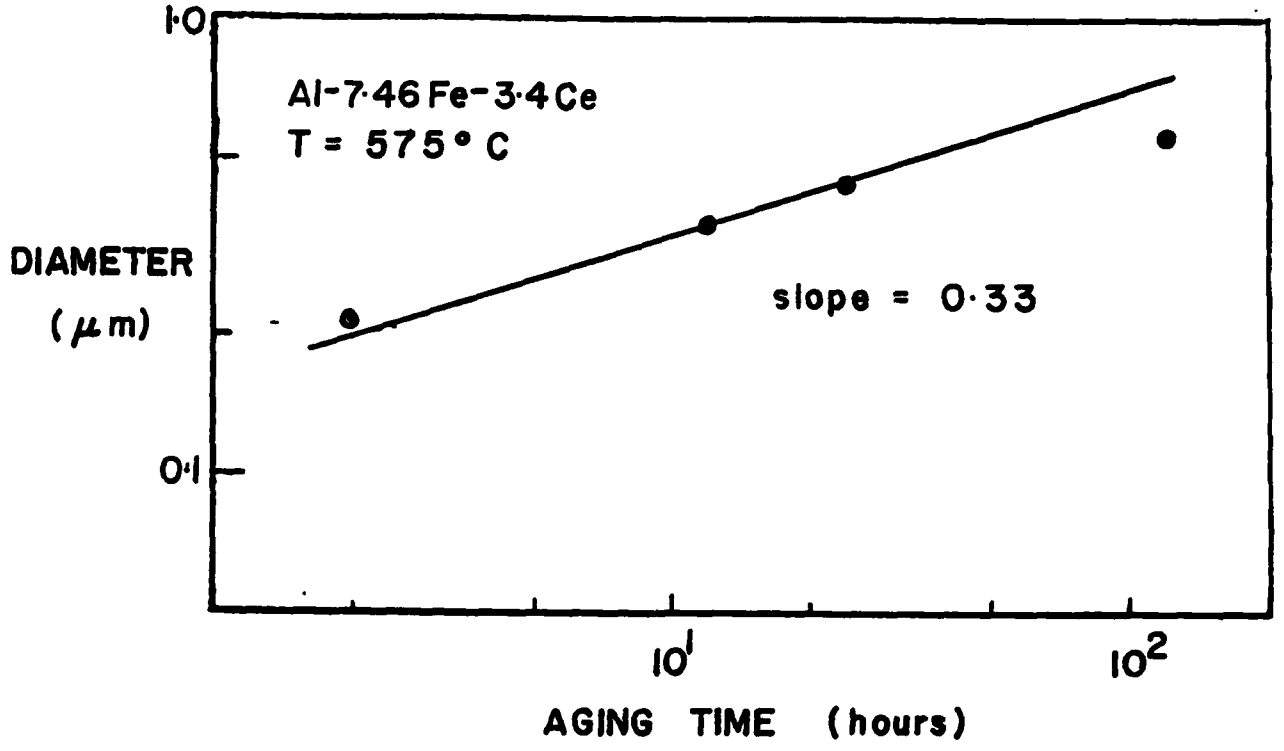

Fig. 5. Log-log plot of the average particle diameter vs. aging time in Al-7.5Fe-3.4Ce aged at 575° C.

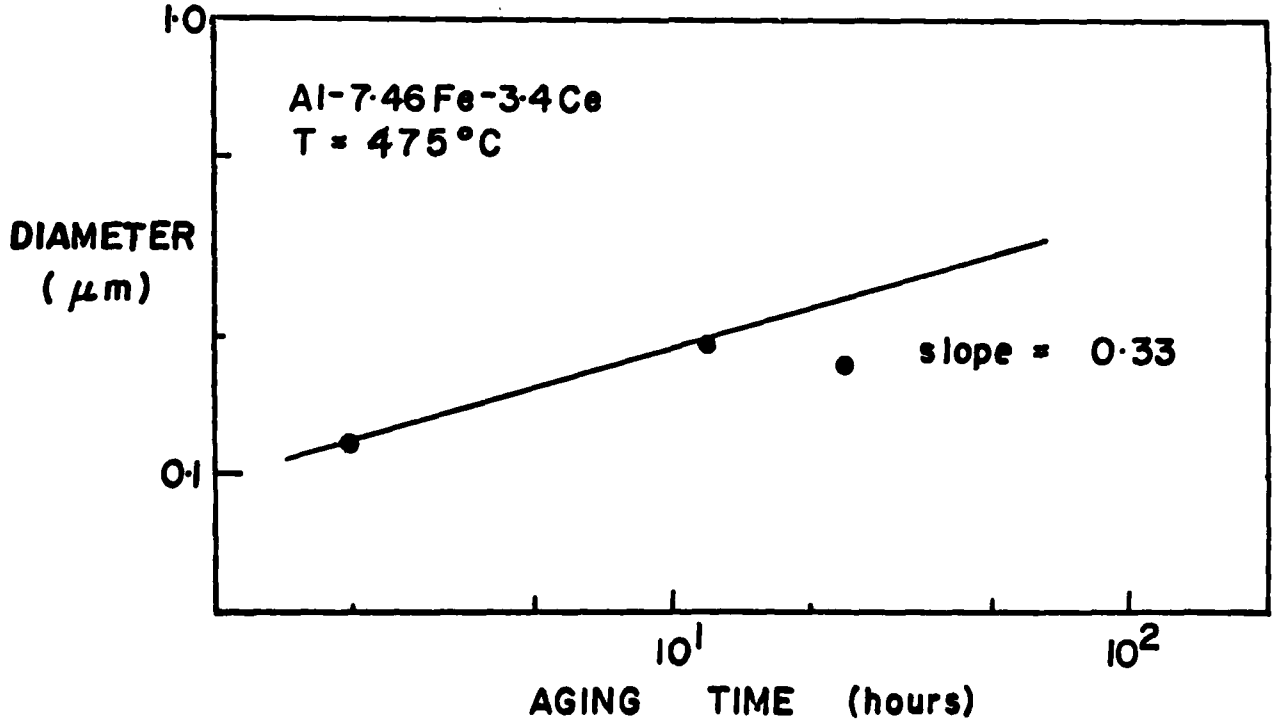

Fig. 6. Log-log plot of the average particle diameter vs. aging time in Al-7.5Fe-3.46Ce aged at 475° C.

(a)

(b)

Fig. 7. TEM micrographs of thin foils of aged Al-7.5Fe-3.4Ce. (a) aged 2 hrs at 575°C, (b) 12 hrs at 475°C.

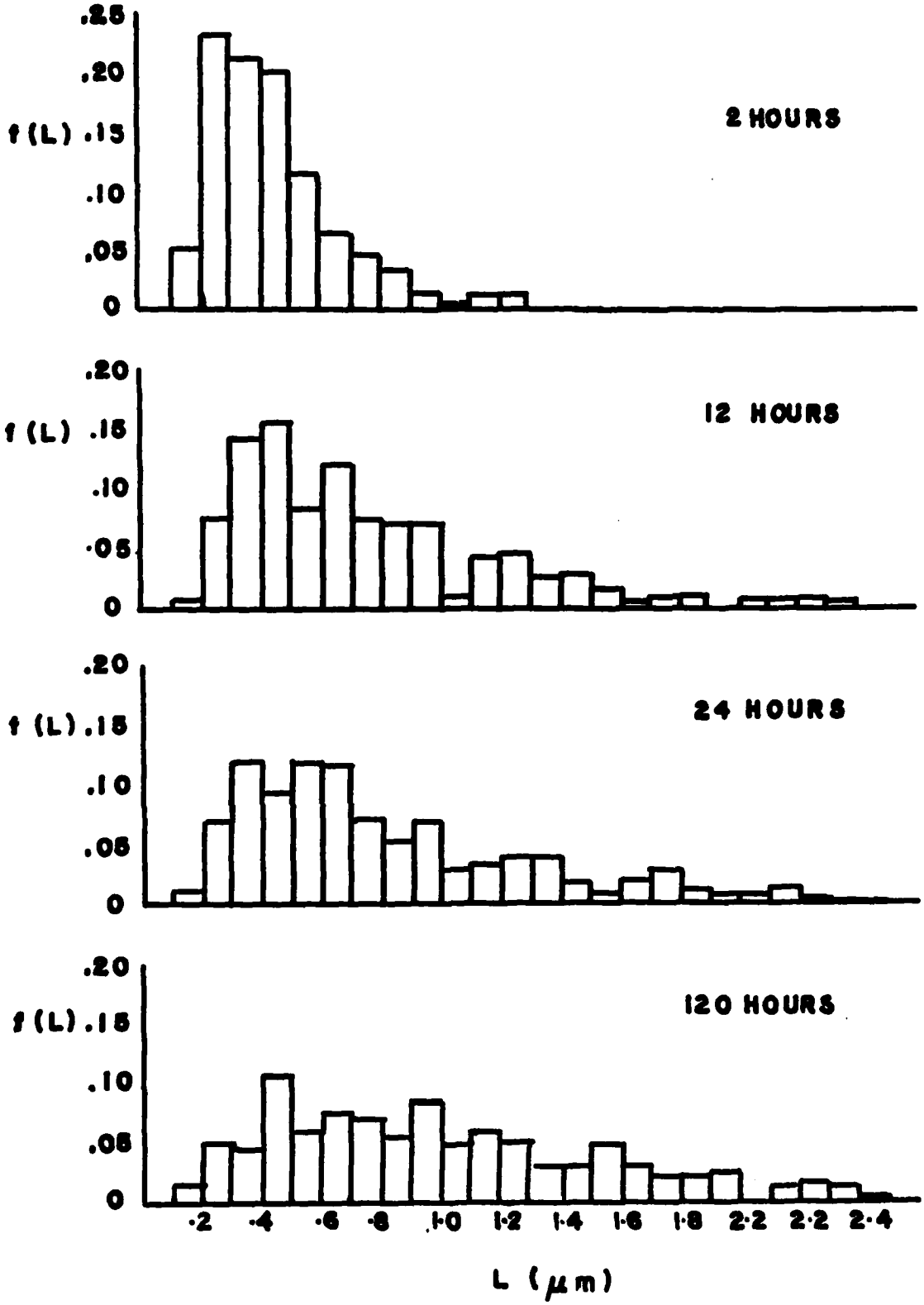

Fig. 8. Histograms showing evolution of the distribution of precipitate size in samples aged at 575° C.

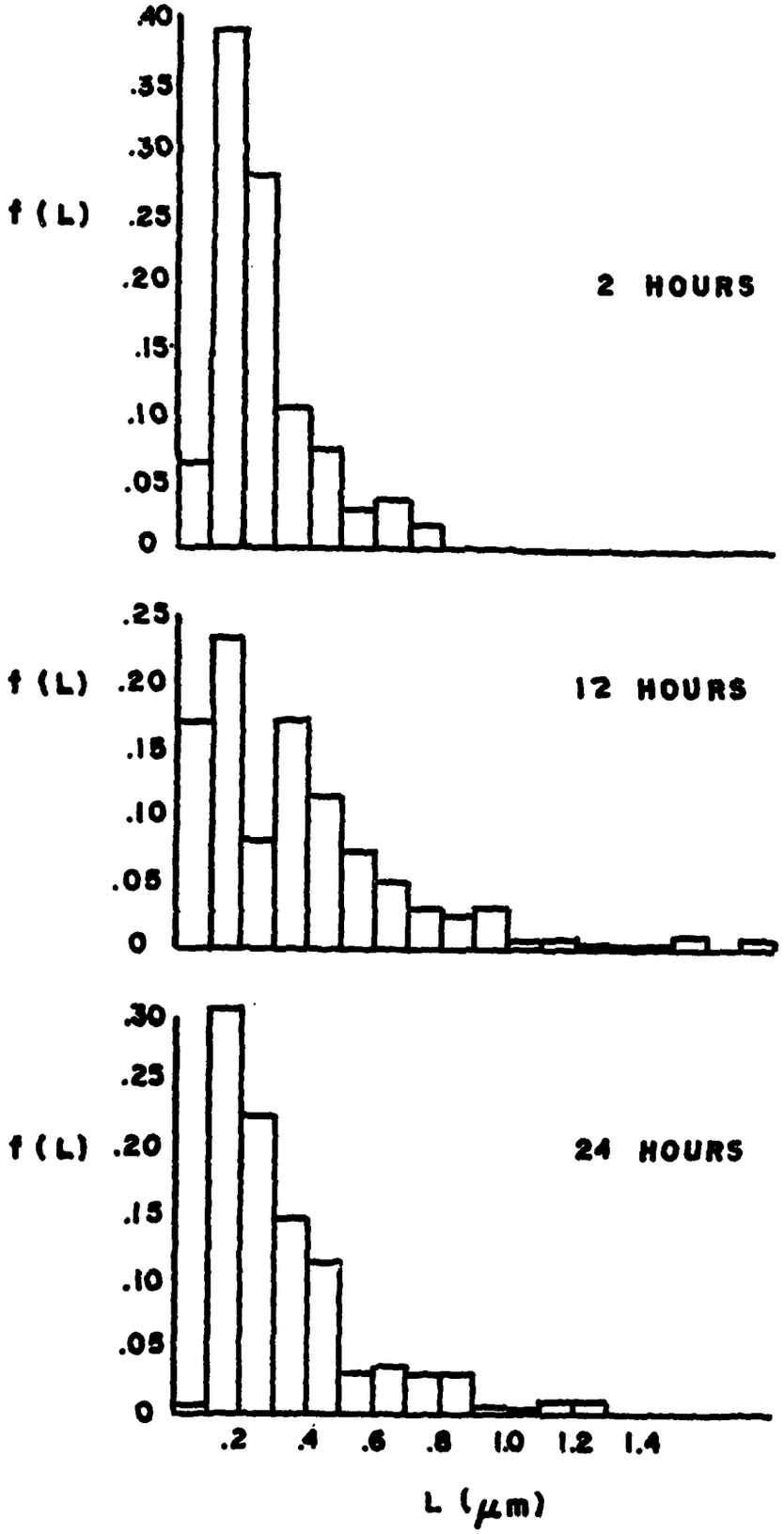

Fig. 9. Histograms showing evolution of the distribution of precipitate size in samples aged at 475° C.

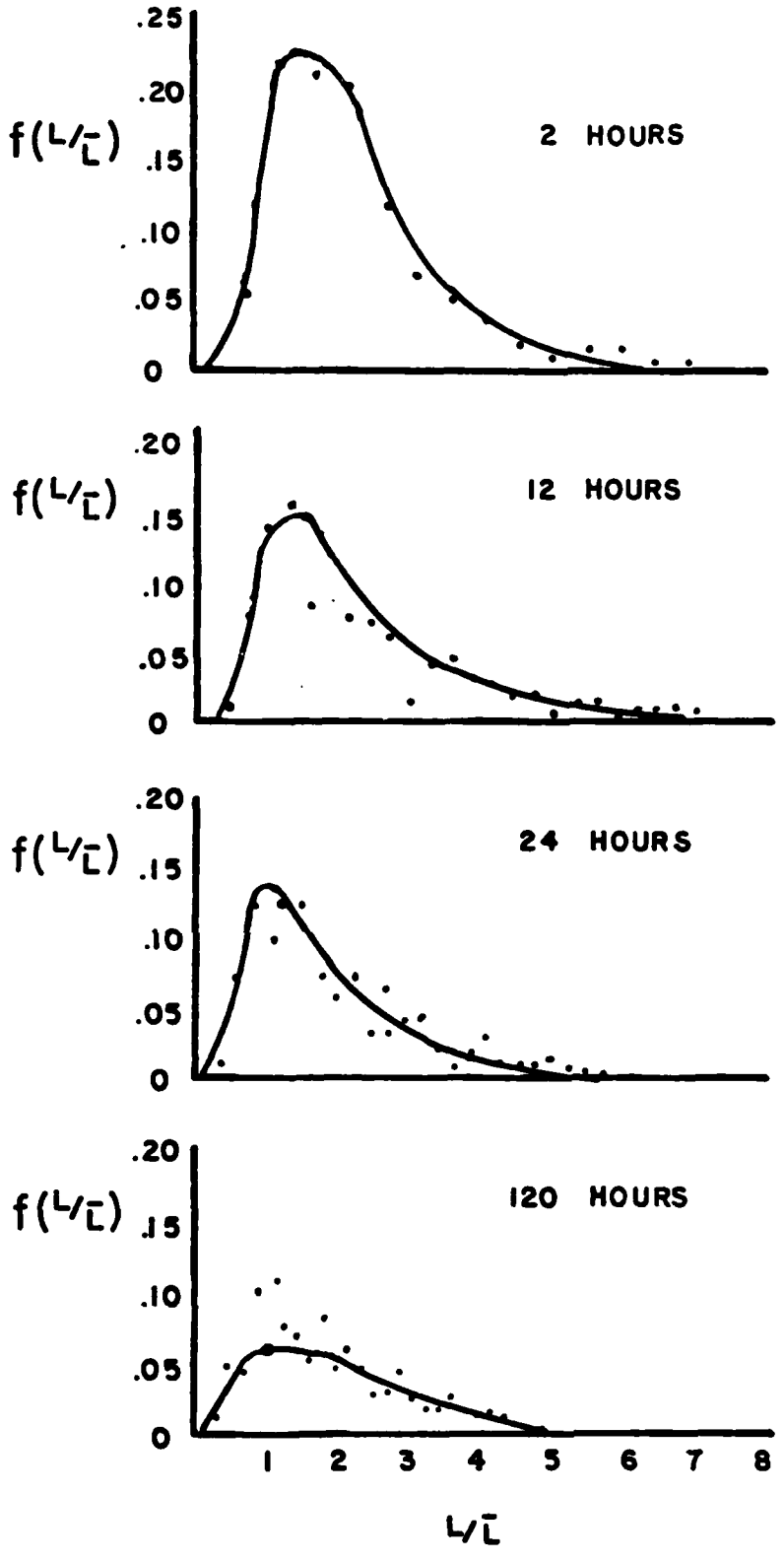

Fig. 10. Frequency of intercept length vs. normalized intercept length in samples aged at 575° C.

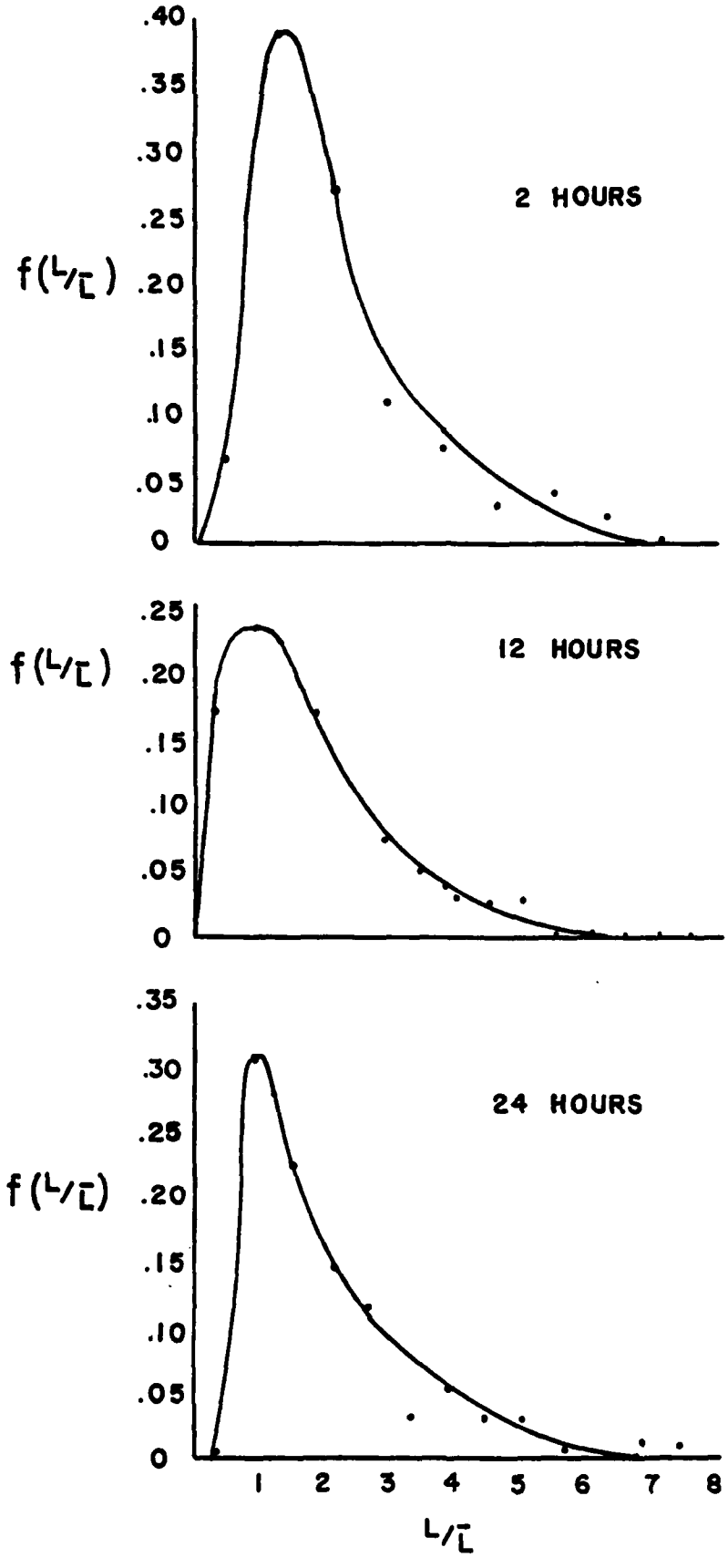

Fig. 11. Frequency of intercept length vs. normalized intercept length in samples aged at 475° C.

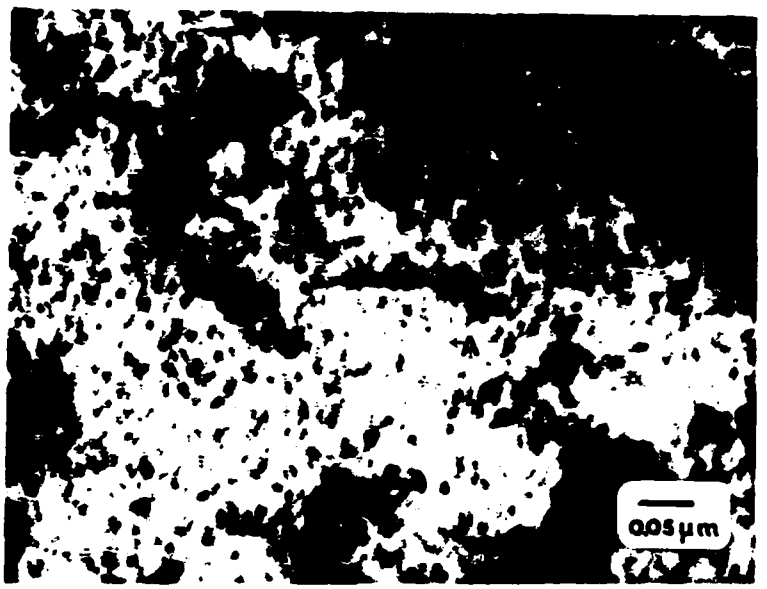

Fig. 12. TEM micrograph of thin foil of Al-7.5Fe-3.4Ce in the as-received condition.

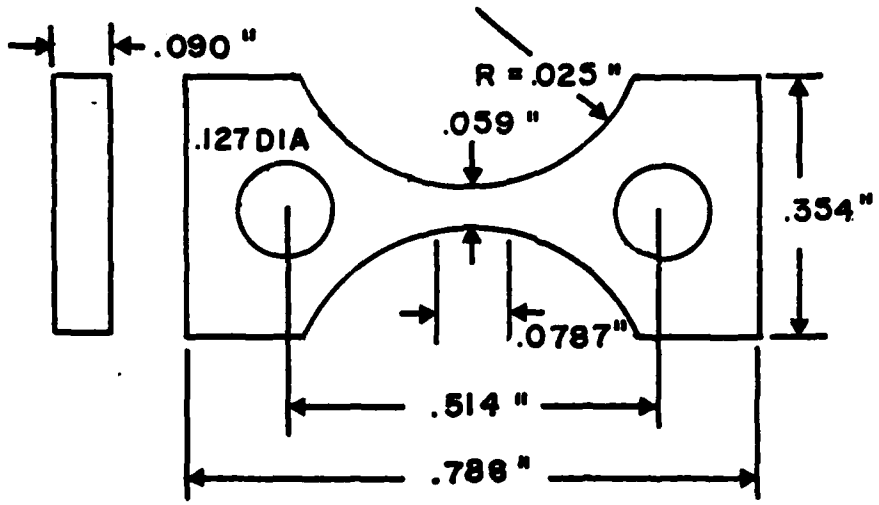

Fig. 13. Geometry of creep specimen.

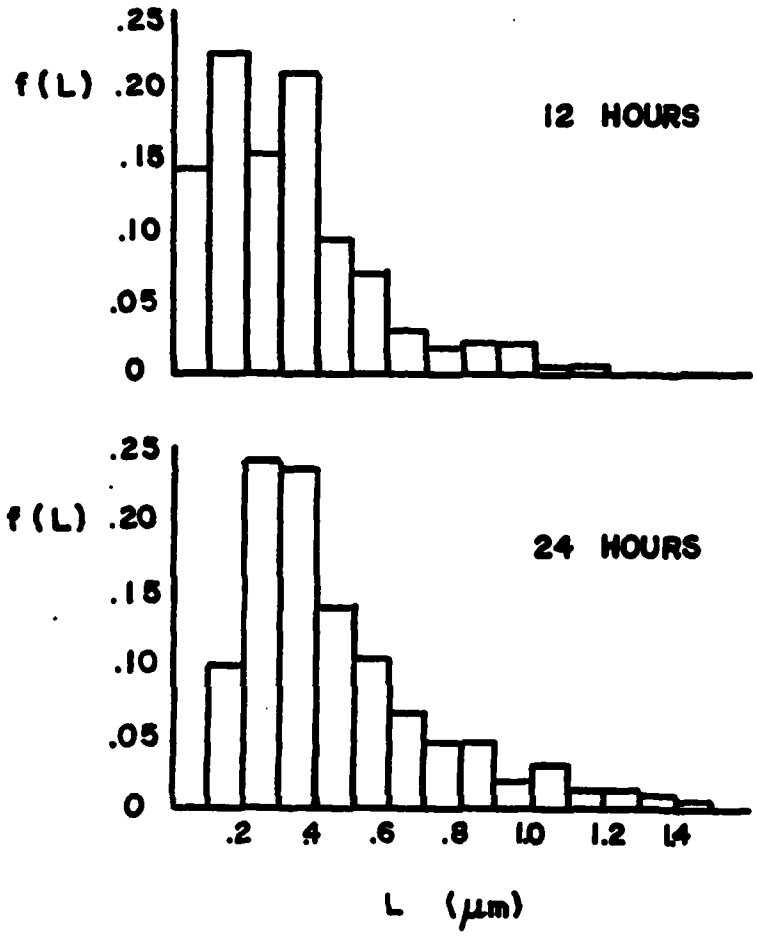

Fig. 14. Histograms showing distribution of precipitate size in samples crept at 1000 psi at 475° C.

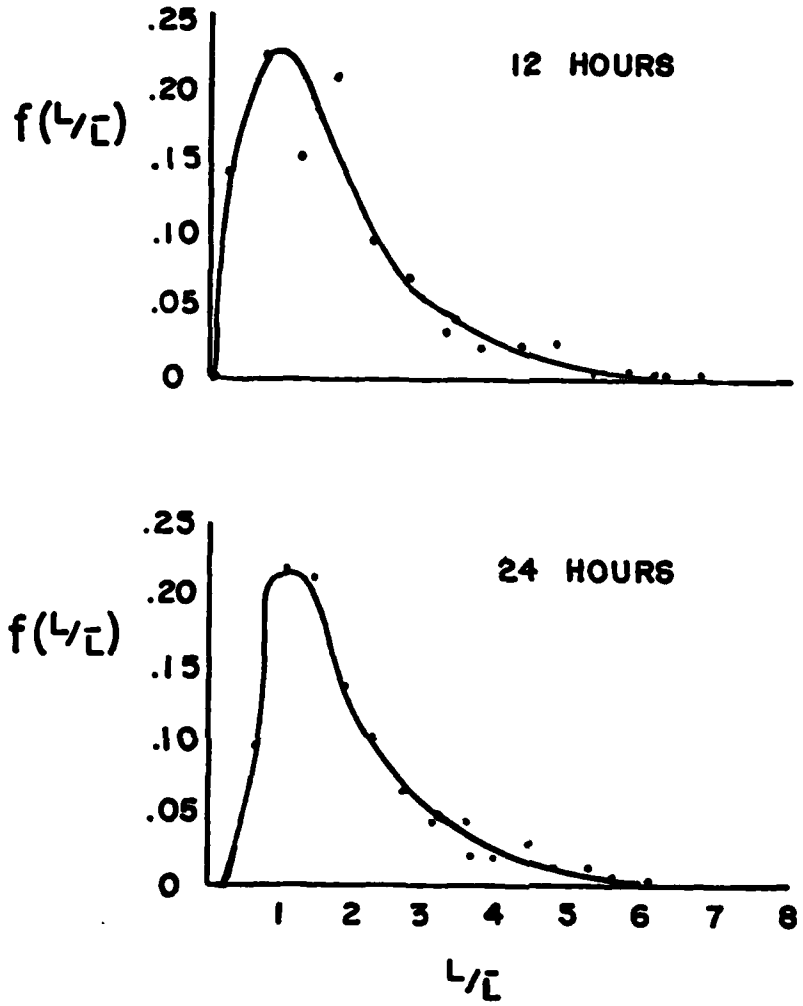

Fig. 15. Frequency of intercept length vs. normalized intercept length in samples crept at 1000 psi at 475° C.

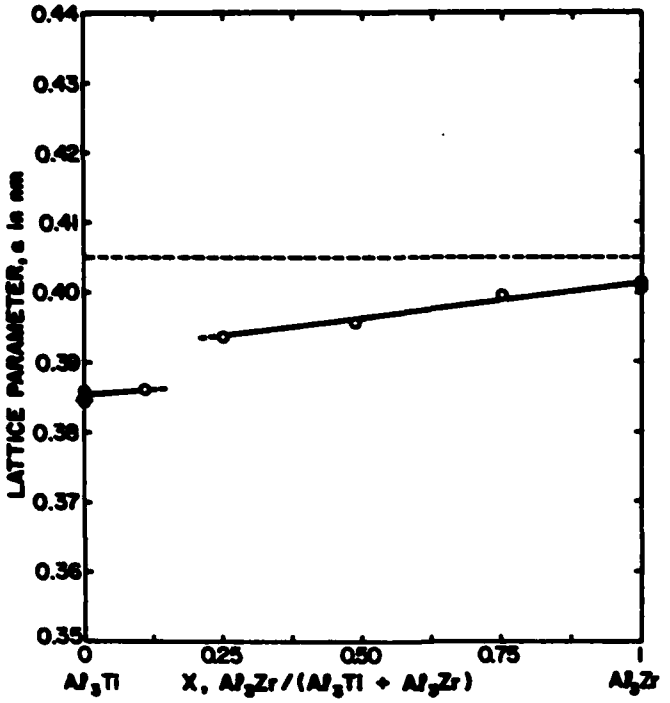

(a)

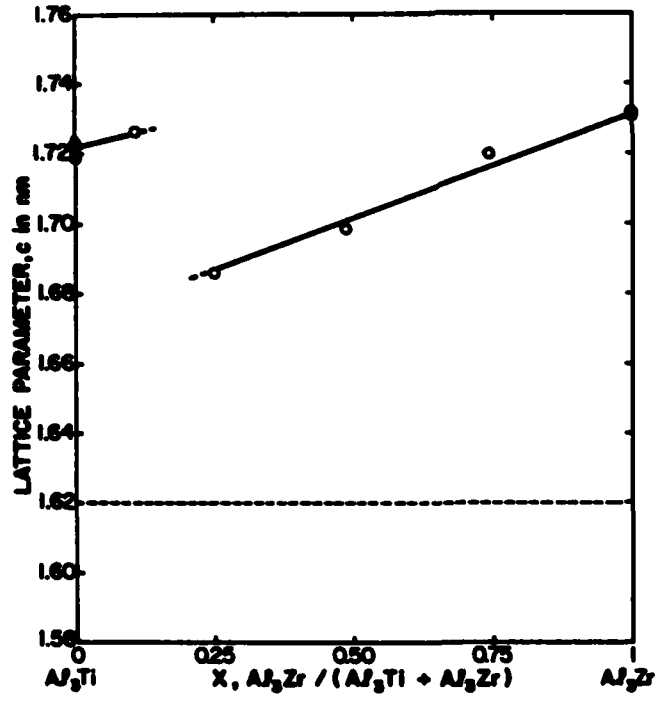

(b)

Fig. 16. Lattice parameters (a) a and (b) c of $Al_3(Zr_xTi_{1-x})$ in Al-2 at.% (Zr+Ti) alloys where c values of the Al_3Ti-type solid solutions are multiplied by 2 for comparison with the c's of the Al_3Zr-type solid solutions; ○ present results, ● JCPDS data, Δ Ar atomized Al-4.7 at.% Ti. Dashed lines are a_o and $4a_o$ of Al solid solutions in (a) and (b), respectively.

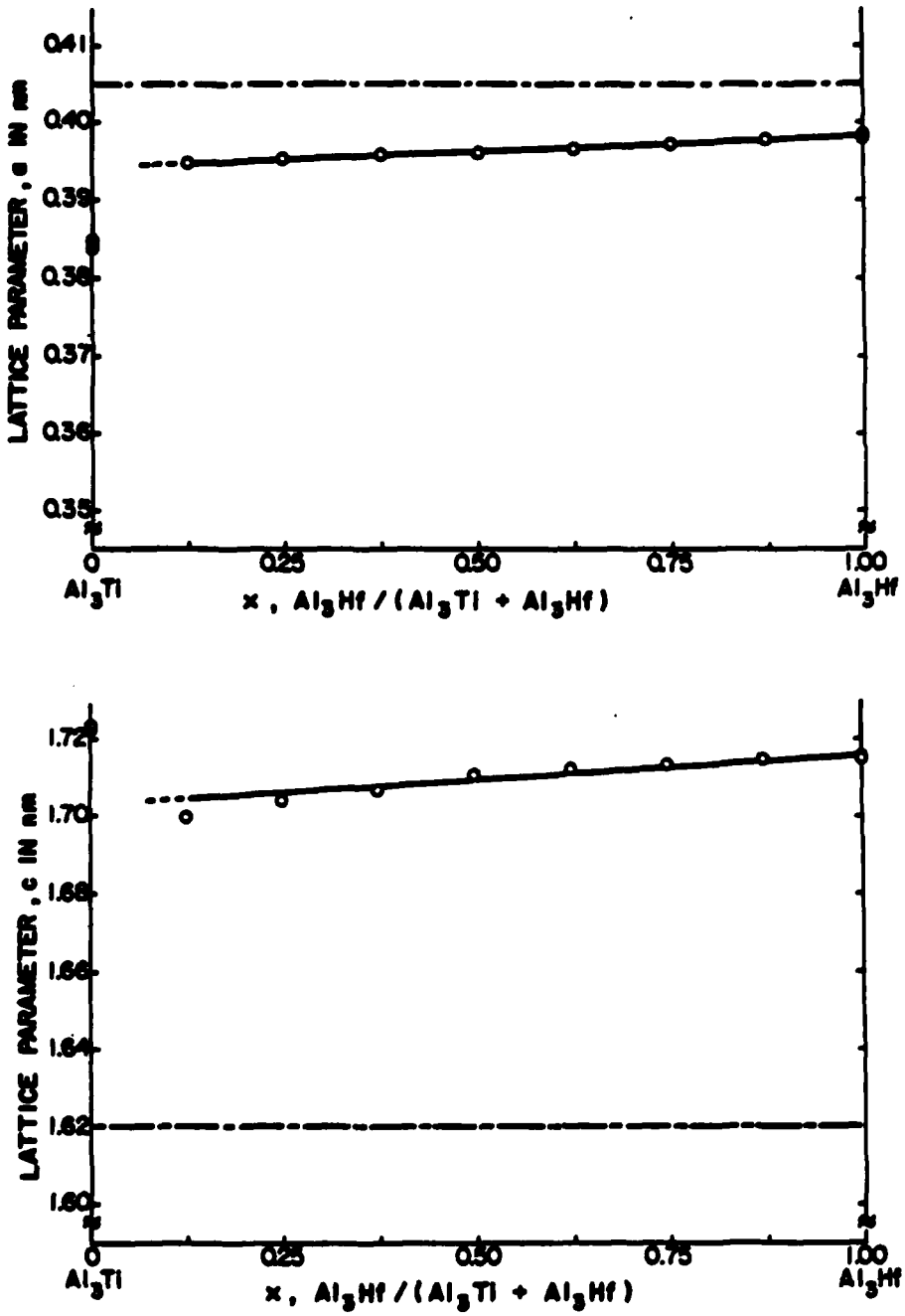

Fig. 17. Lattice parameters (a) a and (b) c of $Al_3(Hf_zTi_{1-z})$ in Al-2 at.% (Hf+Ti) alloys, where c values of the Al_3Ti type dispersoids are multiplied by 2 for comparison with the c's of the Al_3Hf type solid solutions; ○ present results, • JCPDS data. Dashed lines are a_o and $4a_o$ of the Al solid solutions in (a) and (b), respectively.

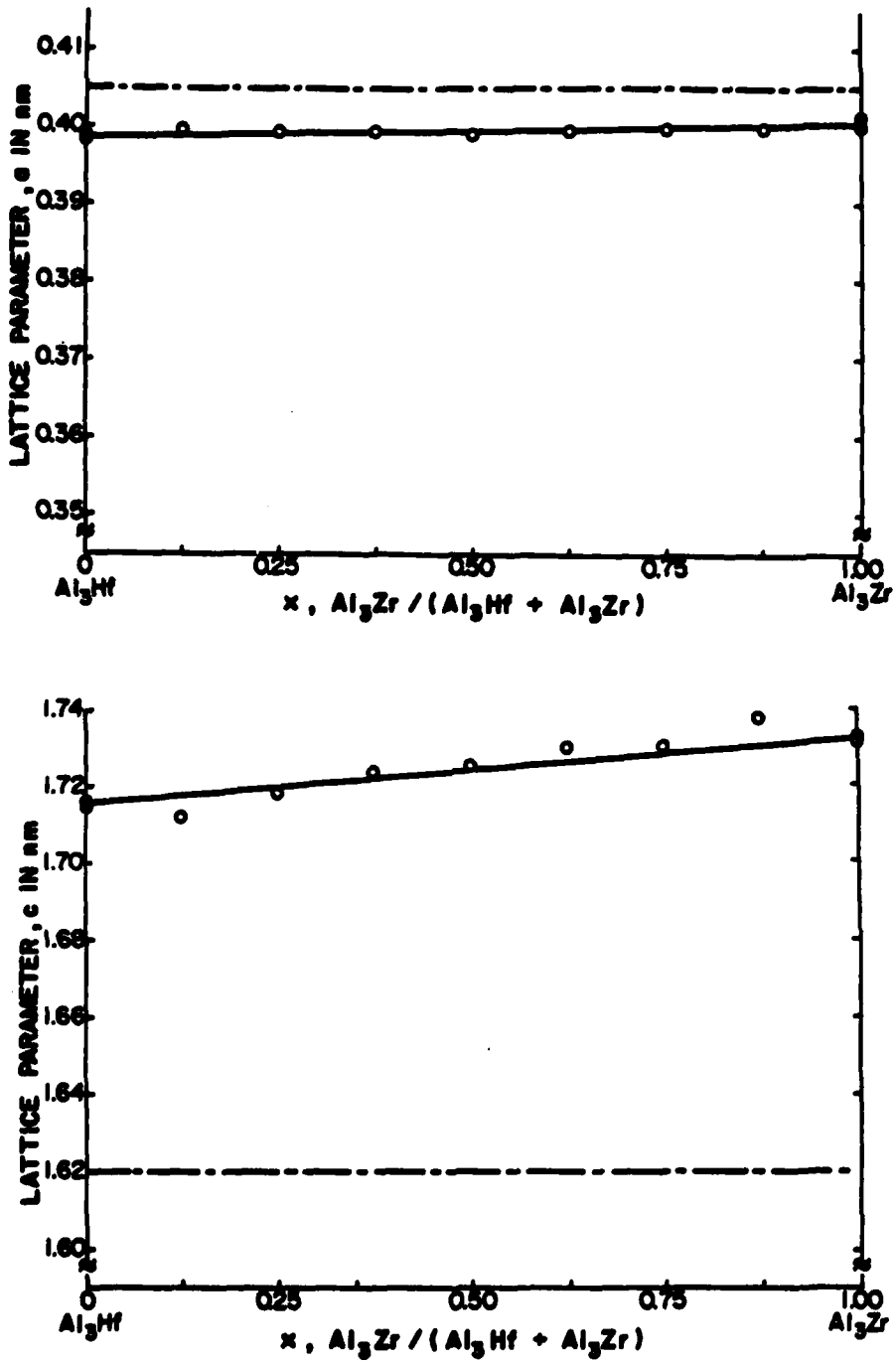

Fig. 18. Lattice parameters (a) a and (b) c of $Al_3(Zr_xHf_{1-x})$ in Al-2 at.% (Zr+Hf) alloys; ○ present results, ● JCPDS data. Dashed lines are a_o and $4a_o$ of the Al solid solutions in (a) and (b), respectively.